PHYSICAL REVIEW RESEARCH **6**, 043193 (2024)

Overcoming photobleaching in imaging of single barium atoms in a solid xenon matrix

M. Yvaine,[1,*] D. Fairbank,[1,*] J. Soderstrom,[1] C. Taylor,[1] J. Stanley,[1] T. Walton,[1,†] C. Chambers,[2,‡] A. Iverson,[1]
W. Fairbank,[1,§] S. Al Kharusi,[2,‖] A. Amy,[3] E. Angelico,[4] A. Anker,[5] I. J. Arnquist,[6] A. Atencio,[7] J. Bane,[8] V. Belov,[9]
E. P. Bernard,[10] T. Bhatta,[11] A. Bolotnikov,[12] J. Breslin,[13] P. A. Breur,[5] J. P. Brodsky,[10] E. Brown,[13] T. Brunner,[2,14]
E. Caden,[15,16,2] G. F. Cao,[17,¶] D. Cesmecioglu,[8] E. Chambers,[7] B. Chana,[18,**] D. Chernyak,[19] M. Chiu,[12] R. Collister,[18]
M. Cvitan,[14,††] T. Daniels,[20] L. Darroch,[2] R. DeVoe,[4] M. L. di Vacri,[6] M. J. Dolinski,[7] B. Eckert,[7] M. Elbeltagi,[18]
R. Elmansali,[18] N. Fatemighomi,[15] B. Foust,[6] Y. S. Fu,[17,¶] D. Gallacher,[2] N. Gallice,[12] G. Giacomini,[12] W. Gillis,[8,‡‡]
C. Gingras,[2] R. Gornea,[18] G. Gratta,[4] C. A. Hardy,[4] S. Hedges,[10] E. Hein,[21] J. D. Holt,[14,2] E. W. Hoppe,[6] A. Karelin,[9]
D. Keblbeck,[22] I. Kotov,[12] A. Kuchenkov,[9] K. S. Kumar,[8] A. A. Kwiatkowski,[14,§§] A. Larson,[23] M. B. Latif,[7,‖‖]
K. G. Leach,[22,¶¶] A. Lennarz,[14,††] D. S. Leonard,[24] H. Lewis,[14] G. Li,[17] Z. Li,[25] C. Licciardi,[26] R. Lindsay,[27] R. MacLellan,[11]
S. Majidi,[2] C. Malbrunot,[14,2] J. Masbou,[3] K. McMichael,[13] M. Medina Peregrina,[25] M. Moe,[28] B. Mong,[5] D. C. Moore,[29]
C. R. Natzke,[22] X. E. Ngwadla,[27] K. Ni,[25] A. Nolan,[8] S. C. Nowicki,[2] J. C. Nzobadila Ondze,[27] A. Odian,[5] J. L. Orrell,[6]
G. S. Ortega,[6] C. T. Overman,[6] L. Pagani,[6] H. Peltz Smalley,[8] A. Perna,[18] A. Pocar,[8] V. Radeka,[12] E. Raguzin,[12] H. Rasiwala,[2]
D. Ray,[2,14] S. Rescia,[12] G. Richardson,[29] R. Ross,[2] P. C. Rowson,[5] R. Saldanha,[6] S. Sangiorgio,[10] S. Schwartz,[10] S. Sekula,[30,15]
L. Si,[4] A. K. Soma,[7,***] F. Spadoni,[6] V. Stekhanov,[9] X. L. Sun,[17] S. Thibado,[8] A. Tidball,[13] T. Totev,[2] S. Triambak,[27]
T. Tsang,[12] O. A. Tyuka,[27] E. van Bruggen,[8] M. Vidal,[4] M. Walent,[16] K. Wamba,[5] H. W. Wang,[17] Q. D. Wang,[31] W. Wang,[19]
Y. G. Wang,[17] M. Watts,[29] M. Wehrfritz,[21] L. J. Wen,[17] U. Wichoski,[16,18] S. Wilde,[29] M. Worcester,[12] H. Xu,[25] L. Yang,[25]
M. Yu,[5] and O. Zeldovich[9]
(nEXO Collaboration)

[1]*Physics Department, Colorado State University, Fort Collins, Colorado 80523, USA*
[2]*Physics Department, McGill University, Montréal, Canada QC H3A 2T8*
[3]*SUBATECH, Nantes Université, IMT Atlantique, CNRS/IN2P3, Nantes 44307, France*
[4]*Physics Department, Stanford University, Stanford, California 94305, USA*
[5]*SLAC National Accelerator Laboratory, Menlo Park, California 94025, USA*
[6]*Pacific Northwest National Laboratory, Richland, Washington 99352, USA*
[7]*Department of Physics, Drexel University, Philadelphia, Pennsylvania 19104, USA*
[8]*Amherst Center for Fundamental Interactions and Physics Department, University of Massachusetts, Amherst, Massachusetts 01003, USA*
[9]*National Research Center "Kurchatov Institute", Moscow 123182, Russia*
[10]*Lawrence Livermore National Laboratory, Livermore, California 94550, USA*
[11]*Department of Physics and Astronomy, University of Kentucky, Lexington, Kentucky 40506, USA*
[12]*Brookhaven National Laboratory, Upton, New York 11973, USA*
[13]*Department of Physics, Applied Physics, and Astronomy, Rensselaer Polytechnic Institute, Troy, New York 12180, USA*
[14]*TRIUMF, Vancouver, Canada BC V6T 2A3*
[15]*SNOLAB, Lively, Canada ON P3Y 1N2*

---

[*] These authors contributed equally to this work.

[†] Present address: Prism Computational Sciences, Madison, WI 53711, USA.

[‡] Present address: TRIUMF, Vancouver, BC V6T 2A3, Canada.

[§] Contact author: fairbank@colostate.edu

[‖] Present address: Physics Department, Stanford University, Stanford, CA 94305, USA.

[¶] Also at: University of Chinese Academy of Sciences, Beijing, China.

[**] Present address: Canadian Nuclear Laboratories, Chalk River, ON K0J 1J0, Canada.

[††] Also at: McMaster University, Department of Physics & Astronomy, Hamilton, ON L8S 4L8, Canada.

[‡‡] Present address: Bates College, Lewiston, ME 04240, USA.

[§§] Also at: University of Victoria, Department of Physics and Astronomy, Victoria, BC V8P 5C2, Canada.

[‖‖] Also at: Center for Energy Research and Development, Obafemi Awolowo University, Ile-Ife, 220005 Nigeria.

[¶¶] Also at: Facility for Rare Isotope Beams, Michigan State University, East Lansing, MI 48824, USA.

[***] Present address: Mirion Technologies, Inc., 800 Research Pkwy, Meriden, CT 06450, USA.

[16]*School of Natural Sciences, Laurentian University, Sudbury, Canada ON P3E 2C6*
[17]*Institute of High Energy Physics, Chinese Academy of Sciences, Beijing 100049, China*
[18]*Department of Physics, Carleton University, Ottawa, Canada ON K1S 5B6*
[19]*Department of Physics and Astronomy, University of Alabama, Tuscaloosa, Alabama 35405, USA*
[20]*Department of Physics and Physical Oceanography, University of North Carolina Wilmington, Wilmington, North Carolina 28403, USA*
[21]*Skyline College, San Bruno, California 94066, USA*
[22]*Department of Physics, Colorado School of Mines, Golden, Colorado 80401, USA*
[23]*Department of Physics, University of South Dakota, Vermillion, South Dakota 57069, USA*
[24]*IBS Center for Underground Physics, Daejeon 34126, Korea*
[25]*Physics Department, University of California San Diego, La Jolla, California 92093, USA*
[26]*Department of Physics, University of Windsor, Windsor, Canada ON N9B 3P4*
[27]*Department of Physics and Astronomy, University of the Western Cape, P/B X17 Bellville 7535, South Africa*
[28]*Department of Physics and Astronomy, University of California, Irvine, Irvine, California 92697, USA*
[29]*Wright Laboratory, Department of Physics, Yale University, New Haven, Connecticut 06511, USA*
[30]*Department of Physics, Queen's University, Kingston, Canada ON K7L 3N6*
[31]*Institute of Microelectronics, Chinese Academy of Sciences, Beijing 100029, China*

(Received 29 June 2024; accepted 4 November 2024; published 25 November 2024)

Neutrinoless double beta decay is one of the most sensitive probes for new physics beyond the Standard Model of particle physics. One of the isotopes under investigation is ^{136}Xe, which would double beta decay into ^{136}Ba. Detecting the single ^{136}Ba daughter provides a sort of ultimate tool in the discrimination against backgrounds. Previous work demonstrated the ability to perform single atom imaging of Ba atoms in a single-vacancy site of a solid xenon matrix. In this paper, the effort to identify signal from individual barium atoms is extended to Ba atoms in a hexa-vacancy site in the matrix and is achieved despite increased photobleaching in this site. Abrupt fluorescence turn-off of a single Ba atom is also observed. Significant recovery of fluorescence signal lost through photobleaching is demonstrated upon annealing of Ba deposits in the Xe ice. Following annealing, it is observed that Ba atoms in the hexa-vacancy site exhibit antibleaching while Ba atoms in the tetra-vacancy site exhibit bleaching. This may be evidence for a matrix site transfer upon laser excitation. Our findings offer a path of continued research toward tagging of Ba daughters in all significant sites in solid xenon.

DOI: 10.1103/PhysRevResearch.6.043193

I. INTRODUCTION

Matrix isolation spectroscopy, the study of atoms and molecules trapped in inert cryogenic crystals, such as solid noble gases, dates to the 1950's. In recent years, there has been increased interest among physicists in simple atoms, atomic ions and molecules in matrices for use in fundamental physics experiments. High density of a doped atom or molecule and long coherence time in the matrix is attractive in searches for the electron elecric dipole moment [1–6] and cosmological axions [7], and for quantum sensing [8]. In the opposite extreme, the capability of imaging single atoms or ions in a cryogenic matrix is critical to some proposed applications. For example, the ability to detect and count individual ^{136}Ba daughter atoms or ions from an extremely rare decay of ^{136}Xe may be crucial for next-generation efforts to observe neutrinoless double beta ($0\nu\beta\beta$) decay [9–32]. This decay probes fundamental properties of neutrinos. A complementary interest is quantum sensing with individual atomic spins [33]. Single atom imaging of ^{25}Mg in solid neon is also being pursued for measurement of the extremely low nuclear cross section of a key reaction for s-process nucleosysthesis, ^{22}Ne(α,n)^{25}Mg [34].

First images of single Ba atoms in solid xenon (SXe) have been achieved [24]. Recently, imaging of single rubidium atoms in a solid neon matrix was reported [33]. A unique aspect of that work was the ability to optically pump and read out the spin state of one atom. These two single atom imaging experiments were done with atoms that experience minimal photobleaching and can scatter $>10^6$ photons before entering a dark state. For high single atom detection efficiency, especially for ($0\nu\beta\beta$) decay, it is important to be able to detect all the desired atoms, even those that bleach more rapidly. In this paper, imaging of single Ba atoms in a second matrix site in solid xenon (SXe) is realized despite significantly faster bleaching, as will be described below, than in the previous work [24].

Although neutrinos were discovered already in 1956 [35], some of their most fundamental properties remain unknown. Neutrinoless double beta decay is a sensitive probe for neutrino properties and new physics beyond the Standard Model of particle physics. If this hypothesized decay were observed, it would demonstrate a process that violates lepton number conservation and confirm that neutrinos are Majorana particles, that is, their own antiparticle. It would also determine the absolute neutrino mass-scale, albeit with uncertainties of a theoretical nature [36]. The EXO-200 experiment, utilizing a liquid xenon (LXe) time-projection chamber (TPC), made the first observation of the Standard Model allowed two-neutrino double beta decay ($2\nu\beta\beta$) in ^{136}Xe [37] and precisely measured its half-life at $2.165 \pm 0.016(\text{stat}) \pm 0.059(\text{sys}) \times 10^{21}$ yr [38]. It also set a limit on the $0\nu\beta\beta$ process in ^{136}Xe of $T_{1/2}^{0\nu} > 3.5 \times 10^{25}$ yr at a 90% confidence level (CL) [39]. A next-generation LXe experiment, nEXO, with 5 tonnes of enriched Xe, is expected to reach a half-life sensitivity to $0\nu\beta\beta$ decay of 1.35×10^{28} yr in a 10 year run [40].

When a double beta decay event occurs in a ^{136}Xe TPC, a ^{136}Ba daughter, that could potentially be identified, is formed at the decay site. The detection of the daughter, referred to as barium tagging, could improve $0\nu\beta\beta$ decay sensitivity by eliminating all backgrounds except those from $2\nu\beta\beta$ [9]. Implementation of barium tagging as a potential future upgrade to nEXO is being investigated by the collaboration. The elimination of all non-$\beta\beta$ decay backgrounds in nEXO could increase the sensitivity by about a factor of 2–3 [40].

One Ba tagging effort in nEXO focuses on extraction from LXe and detection in solid xenon (SXe) [22,24], and another on extraction to gaseous Xe and detection in vacuum [23,25]. Capture of Ba^{++} in a fluorescent molecule is being investigated by the NEXT collaboration for barium tagging for a next-generation gaseous ^{136}Xe double beta decay experiment [26–32].

The principles of the method of Ba extraction in SXe and subsequent tagging have been described previously [22,24]. Briefly, a candidate $0\nu\beta\beta$ decay event is identified by ionization signal characteristics such as total electron energy and multiplicity, and its location in the TPC is determined (see, e.g., Ref. [38]). A cryoprobe is inserted into the TPC, the tip with a sapphire window is cooled below the Xe freezing point, and the potential ^{136}Ba daughter is captured from the decay site in a small volume of solid xenon (SXe) on the window. The probe is extracted from the TPC volume and the LXe to a separate region where the SXe deposit can be cooled to a lower temperature and scanned for the presence of one or zero Ba atoms. Coincident observation of a Ba atom extracted from a candidate $0\nu\beta\beta$ event site provides a positive confirmation of $\beta\beta$ decay.

In LXe, the Ba^{++} daughter from the $\beta\beta$ decay is expected to quickly recombine to form Ba^{+} and mostly remain as such, as the band gap for LXe is less than the ionization potential for Ba^{+} [9]. The best present analog for estimating the final ion fraction for the Ba daughters in LXe is the 76(6)% measured for ^{214}Bi + daughters of ^{214}Pb beta decay [41]. When Ba^{+} is captured into SXe from LXe at thermal energy, 0.014 eV, it is unclear what fraction will remain as Ba^{+} and what fraction will neutralize to Ba by capturing a stray electron. What is known is that both Ba atoms and Ba^{+} ions result from the deposition of 2000 eV Ba^{+} ions into SXe in vacuum [22].

In previous work, the spectroscopy of Ba atoms and Ba^{+} ions in SXe [22,42–44] and first results on imaging of single Ba atoms in SXe [24] have been presented. Theoretical work has identified the geometries of the matrix sites in SXe that give rise to some portions of the observed Ba absorption and emission spectra [44,45]. The 590 nm "blue site" emission (so named in Ref. [44] by the order of absorption band wavelength) is associated with Ba atoms in tetra-vacancy (TV) sites. The 577 nm emission peak has overlapping contributions from Ba atoms in two distinct sites. The 578 nm "violet site" emission is assigned to Ba atoms in asymmetric five- or seven-atom vacancy (5/7V) sites [44,45]. The 577 nm "green site" emission, with an excitation peak between those of the violet site, is associated with Ba atoms in hexa-vacancy (HV) sites [43–45]. The SXe matrix site of the weak 570 nm Ba emission peak is not yet identified. The site for the 619 nm emission is not addressed in published theoretical work, but is attributed to a single-vacancy (SV) site [24,46]. One possible formation mechanism for this less energetically favorable site in our work is the capture of a Ba^{+} ion in a SV site and its later neutralization by recombination with a free electron. The predominant emission lines of Ba^{+} in SXe have also been found experimentally [22], but to date no theoretical results on Ba^{+} in SXe have been published.

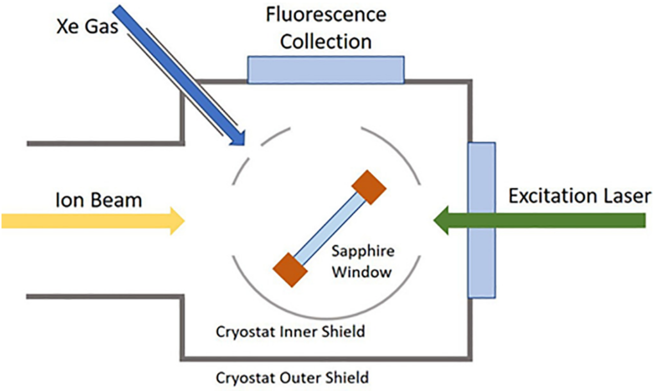

FIG. 1. A schematic diagram of the sample apparatus. The excitation laser enters the vacuum chamber opposite to the Ba^{+} ion beam, and the fluorescence is collected in a perpendicular direction. Xenon gas is directed toward the window by a tube that enters the chamber behind the plane of the diagram.

First images of single Ba atoms in SXe were achieved with SV site Ba atoms emitting at 619 nm [24]. For high-efficiency Ba tagging, it is important to extend single Ba imaging from the SV site to all Ba matrix sites in SXe and to also demonstrate single Ba^{+} imaging in SXe. In this paper, the first step in this extension is presented, imaging of single Ba atoms in a second site, the HV matrix site in SXe using the 577 nm emission peak. Because a Ba atom in this matrix site photobleaches more rapidly than in the SV site [22], single atom imaging is more challenging.

II. EXPERIMENTAL SETUP

The apparatus used in this work is similar to that used for imaging single Ba atoms in SV sites of SXe [24]. A schematic diagram of the sample region is shown in Fig. 1. Matrix samples for the imaging experiments are created on a sapphire window of 0.75 inch diameter [47] that is mounted on the cold finger of a cryostat at a temperature of 50 K. Near the window an inlet tube provides gaseous xenon flow that freezes onto the window to create the matrix sample. In Ba^{+} deposits, pulses of Ba^{+} ions are directed towards the center of the window during the deposition of xenon. The ion pulses begin about 5 seconds after the start of xenon flow and are followed by ∼5 s of xenon deposit after ion deposition is stopped. During implantation, some of the Ba^{+} ions recombine with the ∼20 free electrons that result from ionization of the SXe matrix by each 2000 eV Ba^{+} ion. Thus, a sparse layer of Ba atoms and Ba^{+} ions remains in the middle of a SXe layer of thickness ∼0.5 μm. After deposition, the window and sample are cooled to 12 K for imaging experiments. The window plane is tilted at an angle of about 45° relative to the ion beam so that sample creation, excitation, and fluorescence collection can be done without adjusting the position of the window and the optics.

Since the Ba absorption bands are broad, the choice of laser for imaging of single Ba atoms is not critical. In this work, a Coherent 599 dye laser is used for imaging, while for bleaching studies, the laser is a continuous wave optical parametric oscillator (OPO). The laser illuminates the sample from a direction opposite the ion beam. A laser wavelength of 565.0(1) nm is chosen for near-optimal excitation of HV site Ba atoms and negligible excitation of those in the 5/7V site [44,48]. The typical laser power is 0.4 μW, about two orders of magnitude less than that used for imaging Ba atoms in the SV site, to accommodate the faster fluorescence bleaching of HV site Ba atoms. The laser is focused at the window front surface (toward the ion beam) using an aspheric lens of 7.9 cm focal length to a radius, w, of ∼3 μm. An angled optical flat is used for compensation of the astigmatism of the tilted window.

The resulting fluorescence is collected and collimated by a $f/1.4$ 50 mm focal length NIKKOR camera lens mounted directly above the window. The light is filtered by a Semrock sharp-edged 582 nm bandpass filter with 21 nm FWHM bandpass and an additional tilted 568 nm long pass filter for greater blocking of stray laser light. The combined bandpass transmits the 577 nm peak with high efficiency and some of the 590 nm peak. Because the latter peak has greater bleaching at excitation wavelength 565 nm [22], the contribution of TV Ba atoms to the fluorescence signal is small. The collected fluorescence is steered by two alignment mirrors into a 200 mm focal length camera lens, which focuses the light into an Andor iXON 3 CCD camera. This model features EM (electron multiplying) gain for single photon counting and is held at $-100\,^{\circ}$C. For the experiments reported in this paper, CCD settings of EM gain 300 and preamp gain 1 were used. The conversion factor from counts to detected photons is 12.8 counts/photoelectron, determined by experimental scaling from factory calibration with no EM gain. This value is used in this work. An alternate confirmation of this calibration from the measured slope of the exponential distribution of single photoelectron pulse heights is ∼15 counts/photoelectron.

Movements of the sample window with an amplitude of 13 μm occur during pulses of pressurized helium in the cryostat, so the laser is shuttered with ∼40% duty cycle to minimize this effect. The residual blurring of the laser position relative to single Ba atoms was determined from analysis of images of single Ba atoms in SV sites to be equivalent to effective laser radii of $w_x = 5.73 \pm 0.26$ μm and $wy = 6.62 \pm 0.40$ μm [49] in the plane perpendicular to the laser beam.

The ion source is a commercial Colutron ion gun with E × B mass filter for selecting singly ionized Barium ions at 2000 eV [50]. A series of deflection plates and Einzel lenses provides steering and focusing to deposit the Ba^{+} ions in the center of the window. Typical currents measured by an extractable Faraday cup close to the window were on the order of 5–10 nA. To deposit a small number of ions in a matrix sample, a pair of pulsing plates are set at ±200 V to deflect the beam away from the window. These plates are set to 0 V during pulse periods of ∼1.5 μs to create ion bunches. The induction signal in a set of three disks through which the ions pass provides a monitor of the pulse size during deposits. The effective area of the ion beam was determined to be 6.7 mm^2 prior to the experiments by replacing the window with a Faraday cup. The uncertainty on ion beam density at the window is +20% and −30% [49].

The vacuum is provided by a small turbo pump on a CF2.75” port attached near the cryostat and two larger turbo pumps on CF8” ports attached to the ion beam system. Residual gas levels monitored with a SRS residual gas analyzer are typically around 1×10^{-7} Torr before the cryostat is turned on. Flow of research grade xenon gas (99.995% purity) is controlled with a needle valve for a desired SXe growth rate that has been calibrated by interference fringes. No further purification is used due to the small flow rates used for sample creation.

As in our previous work, to image single Ba atoms we raster scan the focused laser over the sample in steps of 4 μm (transverse to the laser and ion beams) and identify spatially resolved Ba peaks through their fluorescence response. For each laser scan step, the fluorescence signal in counts is determined by summing the counts in a 5 × 5 pixel region centered at the laser position and subtracting a digitizing offset (pedestal) in the CCD readout electronics of 100 counts/pixel. A plot of net counts versus laser x, y position is called a composite image and shows where single Ba atoms are located.

In some of our experiments, the output coupler of the dye laser was adjusted between deposits. This resulted in a shift in the starting y position of some scans of up to six laser steps relative to previous deposits. There were no x position shifts.

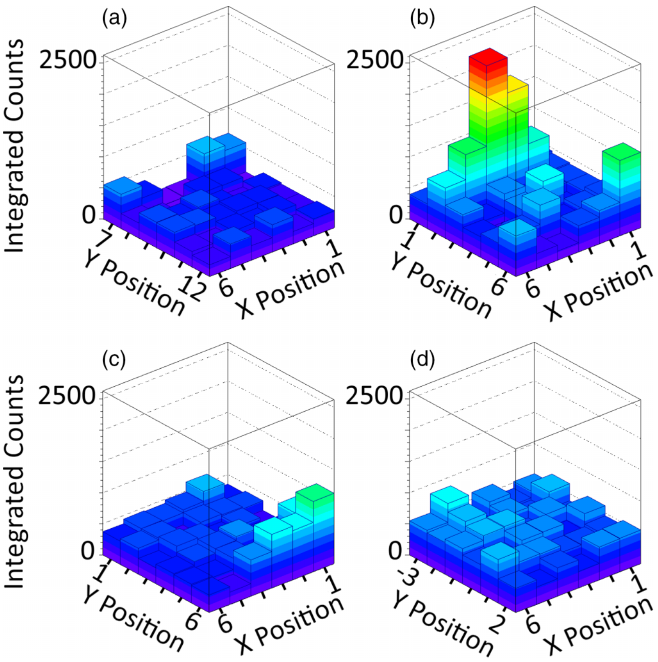

FIG. 2. A set of lego plots of integrated fluorescence counts vs x, y laser position in successive scans from (a) to (d): (a) SXe-only deposit; (b) new SXe with barium deposit, with one distinct peak at laser position (4,2) of the scan; (c) rescan of the SXe with barium deposit in which the prominent feature has photobleached; and (d) new SXe-only after the previous deposit was evaporated. The axes in these plots are rotated 90° clockwise compared to plots shown later in this manuscript for better visibility.

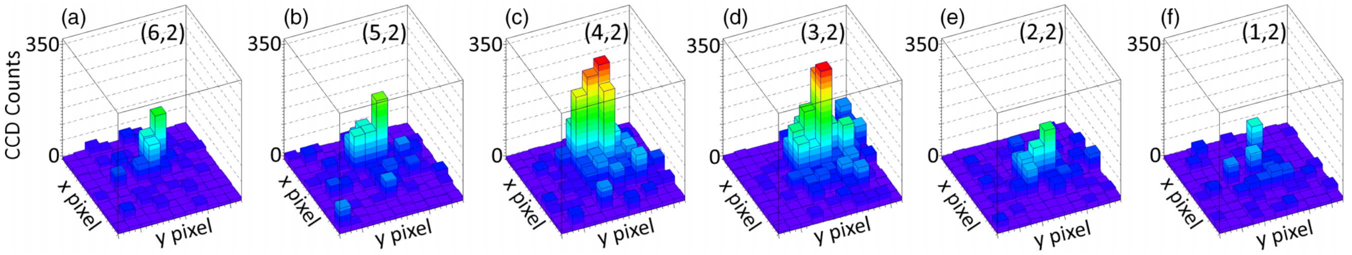

FIG. 3. A set of lego plots of successive 15 × 15 pixel ccd images from the scan depicted in Fig. 2(b). The laser position in scan steps is given in parentheses at the top right of each image. The CCD counts are pedestal subtracted. In the first four images, as the laser passes over the single atom, the fluorescent signal increases, but remains in the same position as the laser moves across. This is an indicator that the fluorescence is coming from a single location in the scan region, rather than being a feature of the moving laser.

III. RESULTS

Results for one set of 6 × 6 step scans with 0.4 μW of laser power for 10 s (25 s × 40% duty cycle) and peak exposure 67 nW s/μm^2 per position are shown in Fig. 2 [51]. Summed fluorescence counts versus laser x, y position are shown for each scan. In (a), a scan over a fresh solid xenon deposit exhibits little signal. In the first two laser positions (1,7) and (2,7), extra background light from the filament of the residual gas analyzer was present, which was turned off by the third position. The average background for the other 34 positions is 281 counts with a standard deviation of 102 counts.

After the Xe-only deposit was evaporated at 100 K, a new Xe deposit with 57^{+12}_{-17} Ba$^+$ ions per scan area (576 μm^2) was deposited at 50 K. In the composite image (b) a single Ba peak stands out clearly above the xenon background with a peak of ∼2600 counts in the frame with the largest signal. The raw images of the laser positions in the second row, (6,2) through (1,2), are displayed in Fig. 3. As the laser moves over the Ba atom, the signal dramatically increases, until vanishing as the laser moves away from that position.

In a second scan of this sample, Fig. 2(c), fluorescence of the single Ba atom is absent, indicating a bleaching of this atom's fluorescence during the exposure of the first scan. It is not clear whether or not the higher signal around laser position (1,6) in scan (b) and rescan (c) of Fig. 2 is from weak excitation of another Ba atom that was just outside the scan area. After the second scan, the deposit was evaporated and a new xenon-only deposit was made and scanned. No significant fluorescence peaks were observed in this SXe-only scan, Fig. 2(d).

Other experiments were done with the same laser power, 0.4 μW, but reduced laser exposure time, 2.5 s per position, to reduce the amount of photobleaching of the candidate peaks during a scan. One purpose of these experiments was the possible observation of the fluorescence turnoff of one Ba atom.

The composite 12 × 12 step scan images of a Xe-only deposit and a subsequent set of scans of a Ba deposit in SXe are shown in Fig. 4. Lower exposure resulted in fewer photons detected, 6 on average per position in the Xe-only scan (a), resulting in higher relative statistical fluctuations. After the scan, the Xe-only deposit was evaporated and another deposit of xenon with 326^{+65}_{-98} Ba$^+$ ions in the scan area (2304 μm^2) was made, scanned and then rescanned. Results are shown in (b) and (c). A potential single Ba atom candidate is present in both the Ba scan (b) and rescan (c) at position (6,10) with a peak of ∼360 counts in (b) and ∼400 counts in (c).

Since the fluorescence signal of this potential single Ba atom candidate persisted on rescan, the laser was then moved

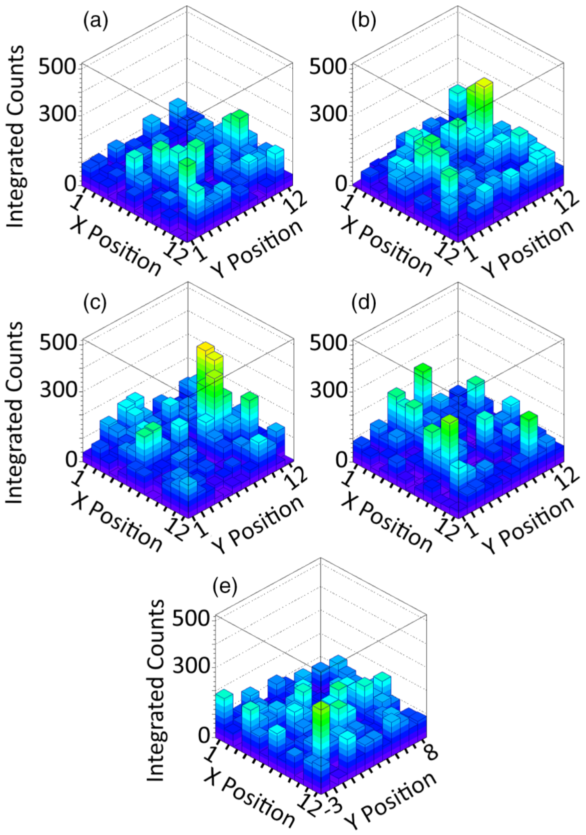

FIG. 4. Lego plots of a successive set of deposits and composite scans with lower exposure time: (a) SXe-only deposit and scan; (b) SXe deposit with barium which has a few higher features compared to (a); (c) rescan of the same deposit in which the strongest feature in (b) persists; (d) another rescan of the same deposit as in (b) and (c) after exposure for 50 frames on the feature of interest at position (6,10); and (e) SXe-only deposit with a similar average signal level as in (a). A laser alignment between scans (d) and (e) resulted in a −4 step y-position shift.

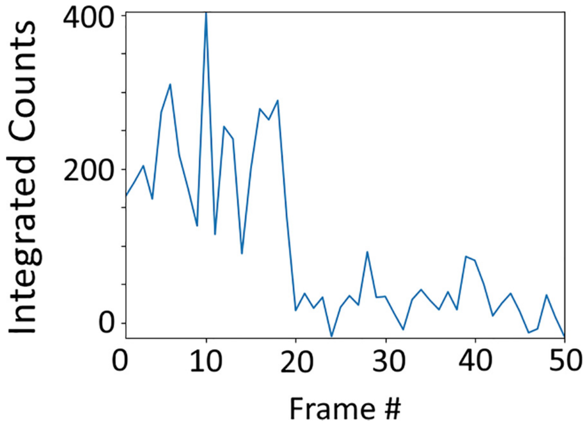

FIG. 5. Signal vs time from 50 frames with the laser at position (6,10) of the Ba feature that persisted in Figs. 4(b) and 4(c). Each frame had 2.5 s of 0.4 μW laser power.

to position (6,10). 50 CCD frames were taken in this location at the same level of exposure as in the scan. The integrated signal for each of the 50 frames is shown in Fig. 5. For the first 19 exposures there was an average of 215 ± 18 counts detected per frame; then the signal abruptly dropped to an average of 26 ± 5 counts detected per frame. Such a turn-off to background level is a strong indicator of fluorescence from a single Ba atom. While the turnoff time is comparable to that of the Ba atom in the SV site (30 s) in Ref. [24], it occurs at about two orders-of-magnitude less exposure due to the 100x difference in laser power in the two experiments. In a subsequent rescan of the area, Fig. 4(d), the Ba atom signal was absent at position (6,10), as expected. After this deposit was evaporated, another Xe-only deposit was made and imaged in Fig. 4(e). The average signal had around 7 detected photons per position, only slightly higher than in the first Xe only deposit of Fig. 4(a). Both Xe-only scans are visibly lower in signal and variations than the three scans of the deposit with barium.

The apparent discrepancy of ∼2 photons/frame "off" background level in Fig. 5 with 6-7 photons/frame background in the Xe-only scans of Figs. 4(a) and 4(e) is also found in other experiments. For example, in four Xe-only scans and seven "spot sits" with fixed laser position on this day and the next day, the spot-sit "off" signals were consistently smaller and ∼40% of the Xe-only averages. A possible mechanism is partial photobleaching of the background that is not observed in individual frames due to low photon statistics.

Lego plots of averages of the raw pedestal-subtracted CCD images of first 19 frames ("on") of the run in Fig. 5 and of the latter 31 frames ("off") are shown in Figs. 6(a) and 6(b), respectively. A clear image of a single Ba atom is seen in (a). To confirm that the turnoff of atom fluorescence is not as a result of laser movement, two-dimensional plots of these averages are shown in Figs. 6(c) and 6(d), with a 4x magnified intensity scale in (d). The small background signal from surface fluorescence in the latter 31 frames lies at the lower end of a weak line of fluorescence from a very low concentration of Cr^{3+} ions in the bulk of the sapphire window [52]. The surface background is at the same position within 0.5 pixel as the laser fluorescence signal of the former 19 frames (marked by a circle). This confirms the absence of *xy* motion of the laser. Technically, *xy* motion of the window in its plane that carries the Ba atom out of the laser beam, cannot be excluded by this method. However, the sudden turnoff and the absence of an atom signal at a shifted position in the rescan strongly suggest that the window did not move.

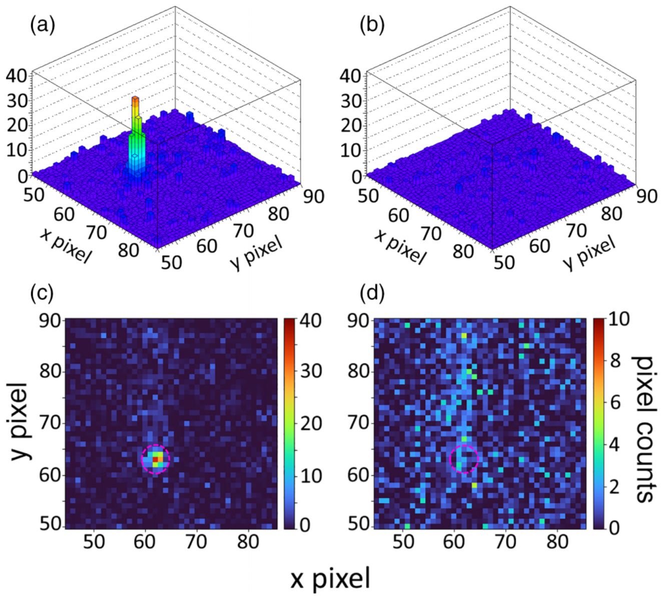

FIG. 6. Lego plots of (a) the average of the first 19 frames of Fig. 5 at position (6,10) (fluorescence "on") and (b) the average of the remaining frames (fluorescence "off"); 2D intensity plots show laser position: (c) first 19 frames and (d) remaining frames rescaled 4x.

IV. DISCUSSION

A comparison of the images obtained of SV site Ba atoms [24] and those in HV sites in this work illustrates the need for characterizing, understanding and mitigating photobleaching. Theoretical understanding is difficult in part because many absorption-emission cycles (10^3 to $>10^7$) occur before some bleaching mechanism terminates the process. In addition, in multivacancy sites in SXe, the smaller excited ^1P state Ba atom likely wanders around the larger SXe hole in the few ns before it emits, as was found in simulations of excited Na atoms in TV sites in solid krypton [53].

Reversible fluorescence wavelength change due to transfer between thermally stable matrix configurations has been observed for Yb in SAr [54]. Site transfer has not yet been identified as a major bleaching mechanism for Ba in the HV site, although first evidence for transfer from the TV site to the HV site is presented below. Because recovery in dark from bleaching has not been observed, even over hundreds of seconds, optical pumping to metastable D or $^3P_{0,2}$ states, as would occur in vacuum, is not a bleaching mechanism. In a non-symmetric diatomic BaXe environment, metastable state lifetimes are significantly reduced because the parity selection rule of atoms is modified by Stark mixing [55]. Chemical reactions with rare impurities in the matrix are minimized by

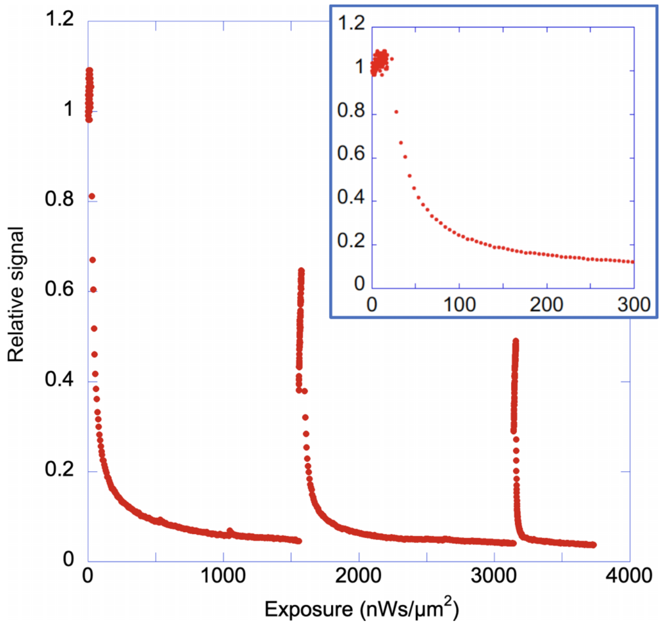

FIG. 7. Normalized 577 nm Ba fluorescence vs. exposure for a large Ba deposit. Recovery of fluorescence during two subsequent sample anneals to 40 K in the dark can be seen. The inset shows an expanded view of initial bleaching of this Ba deposit during the first 300 nW s/μm^2.

forming the matrix at 50 K, which is above the condensation temperature of N_2, O_2 and H_2 in vacuum.

Results of a bleaching experiment with a large Ba deposit, ~5 s of DC Ba^+ beam, and a defocused laser beam at 565 nm with $w_x = 258$ μm and $w_y = 315$ μm from a continuous-wave optical parametric oscillator (OPO) are shown in Fig. 7. Fluorescence was passed through a spectrometer to produce successive Ba emission spectra. The combination of a narrow spectrometer slit compared to w_x and a narrow y integration range compared to w_y assures uniform laser intensity in the region sampled. As shown in the inset, in the first 100 frames, with 0.09 nW/μm^2 laser intensity and 2 s exposure time (18 nW s/μm^2), a slight antibleaching occurs in the 577 nm fluorescence peak of HV site Ba atoms. During this period, the 590 nm fluorescence peak for TV site Ba atoms bleaches by about a factor of 2. Sample spectra are shown in Fig. 8(a).

The next 300 frames were taken with 1 s exposure time and a laser intensity 5.1 nW/μm^2 that is close to the central intensity of the focused laser beam in the experiments of Figs. 2–6, 6.7 nW/μm^2. The 577 nm fluorescence in these frames decays rapidly initially and then slowly at longer exposures. It can roughly be described by a power law of exponent −0.6 or a double exponential plus a constant with a faster and a slower exponential decay.

Two possible interpretations of the decay behavior of the bleaching curve in Fig. 7 are that (1) bleaching is an inhomogeneous process with fluorescence turnoff time different for different Ba atoms and (2) bleaching involves a homogeneous process with Ba atoms making semi-reversible transitions between multiple matrix sites with certain rate constants. In the inhomogeneous interpretation (1), the fluorescence of the Ba atom in Fig. 2 with average total exposure 250 nWs/μm^2 per scan has 13% probability of survival based the beaching curve in Fig. 7. For the Ba atom in Fig. 4 with 1/4 as much exposure per frame, single Ba fluorescence lasting one scan has about 30% probability. The fluorescence of the Ba atom in Figs. 4 and 5 that lasted through two scans and 19 "spot sit" frames before turnoff with exposure 440 nWs/μm^2 has about 10% probability. The homogeneous process (2) has been observed for Yb atoms in solid argon. A rate equations fit shows more rapid reversible transfer between the "violet" (HV) and "blue site" (TV) peaks and a slow increase in the "red site" (SV) peak [54]. One of the interesting predictions of this model is that if observations could be made at the single atom level "blinking" back and forth at the HV and TV emission wavelengths may be observed before slow turnoff to the SV site emission. This model applied to our data for Ba in SXe has three matrix states, the HV site and two other states that have not yet been determined. The five constants in the double exponential plus constant fit are not sufficient to determine the

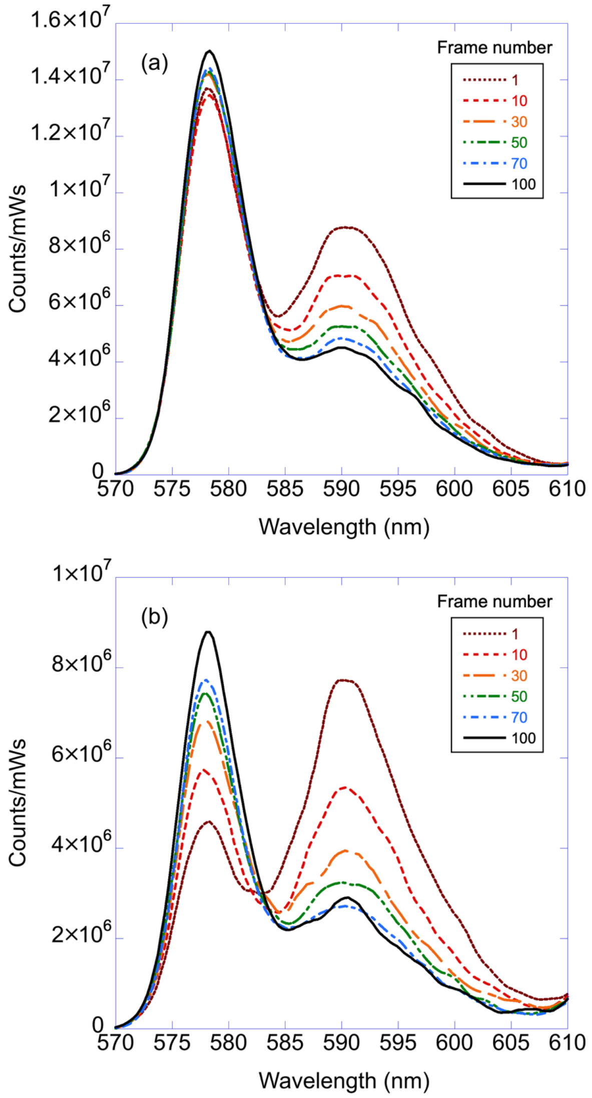

FIG. 8. Selected spectra in the first 100 frames (a) on a new deposit and (b) after the first anneal following a large exposure. These spectra show antibleaching of the 577 nm peak and concurrent bleaching of the 590 nm peak.

six decay rates and three initial populations in the model. Two qualitative comments may be made. First, the sum of the slow and fast decay rates, 0.05 $(\mathrm{nW\,s}/\mu\mathrm{m}^2)^{-1}$, is the sum of all six population transfer rates in the model and gives an upper limit on the fastest blinking rates. The single Ba fluorescence that lasted 19 frames in Fig. 5 might have included some blinking, but the low photon statistics of the data make a resolution of blinking challenging. Second, the constant in the fit is proportional to the return rates from state 3 (the γ's in the Tao model), and its nonzero value indicates that some blinking could occur on greater exposure scales. Additional studies of bleaching as a function of temperature, laser intensity and wavelength, both with many Ba atoms and at the single atom level, would be useful to clarify the bleaching process and to optimize conditions for efficient single Ba atom imaging.

Recovery from excitation-induced transfer from one matrix site to another by annealing has been reported for Yb and K in SAr and Ag in SXe [54,56,57]. Such a process is also observed for Ba in SXe in Fig. 7. Following the bleaching run in the first 1559 $\mathrm{nW\,s}/\mu\mathrm{m}^2$ of Fig. 7, the sample was annealed in the dark to 40 K and returned to 12 K over 10 minutes. An immediate recovery to about 40% of the original 577 nm signal was observed. Over 100 low intensity frames, antibleaching of 577 nm peak increased the recovery to 65% while the 590 nm fluorescence bleached significantly. Sample spectra from this run are shown in Fig. 8(b). In the runs to this point the x and y positions of the OPO laser were steady as monitored by the y position and intensity of the 619 nm peak for SV site Ba atoms that bleach little under these exposures. Thus, for these cases, the recovery is not due to movement of the laser to less bleached Ba atoms. After further bleaching, as much as half of the original signal returned on a second annealing cycle while the sample was not exposed. During the second bleach, a little flattening of the bleaching curve is observed at the bottom due to y movement of the laser beam at that time of magnitude 0.4 times the laser radius w. Otherwise, laser motion did not significantly change the exposure in these runs. Further investigation is planned to see if annealing could be utilized to extend fluorescence duration and increase the number of detected photons per atom. This could enhance the efficiency and validation for imaging of single Ba atoms in HV sites.

V. CONCLUSIONS

A key technology in a Ba tagging scheme for ^{136}Xe neutrinoless double beta decay searches is the ability to identify and count single atoms in solid xenon. While single Ba imaging was previously demonstrated for barium atoms in SV sites in solid xenon, the ability to do this for Ba atoms in other matrix sites that experience greater photobleaching is critical. The first such images of single Ba atoms in the HV site are presented in this work. Sudden fluorescence turnoff of one Ba atom with particularly long fluorescence duration was observed.

Thus far, the percentage of Ba$^+$ ions deposited into SXe in vacuum and imaged as single Ba atoms is in the few percent range for both SV and HV sites. This ratio includes an unknown fraction of Ba$^+$ ions neutralized to Ba in present experimental conditions. In the former case, a limiting factor may be low population of the energetically disfavored SV site. For Ba atoms in the HV site a method to overcome photobleaching would be helpful. The observed 2/3 recovery of fluorescence for the 577 nm line by annealing is a promising step in this direction. The conversion of Ba atoms from the faster bleaching TV site of SXe to the HV site, in which single Ba imaging has been demonstrated here, is a hopeful avenue to explore further toward counting of the Ba atoms that are initially in TV sites. The SV, TV, HV and 5/7V sites constitute the major configurations of Ba in SXe observed in our work. Research is also underway in our laboratory on single Ba$^+$ imaging in solid xenon. In liquid xenon, it is not known into which of these sites the daughter Ba atoms and Ba$^+$ ions from double beta decay will be captured when frozen into SXe. Initial studies are ongoing in our group. Measurement of the Ba-ion fraction following radioactive beta decay of Cs, for example, ^{136}Cs to ^{136}Ba, ^{138}Cs to ^{138}Ba, or ^{139}Cs to ^{139}Ba, would provide additional insights into the expected Ba/Ba$^+$ fraction following a double beta decay. Ultimately, efficient single Ba and Ba$^+$ imaging in all sites is desirable to investigate. In this regard, a significant step forward has been presented in this work.

This Ba tagging method may, in principle, be applicable to a gaseous xenon detector. Techniques being developed by the NEXT collaboration could be used to guide and concentrate the Ba^{++} daughter ion into a smaller gas volume from which it might be captured in solid xenon on a cryogenic window. As in LXe, when Ba^{++} enters SXe, it should spontaneously recombine with one conduction band electron due to similar LXe and SXe bandgap energies. After extraction of the cryoprobe, detecting the Ba$^+$ or Ba (if further neutralization occurs) by single atom or ion imaging could be done by the methods discussed in this work. Of course, many technical issues will be different and would need to be studied. A solid xenon detector has also been proposed and initial feasibility studies have been done [58]. In SXe, the Ba$^+$ daughter would remain at the decay position. In principle, the techniques of single Ba and Ba$^+$ imaging in SXe being developed in our laboratory might be applied from a greater distance in the bulk detector in an in-situ manner similar to that proposed by Moe [9]. The gradual accumulation of Ba daughters from $2\nu\beta\beta$ decay would have to be overcome. A method for more permanent bleaching of Ba/Ba$^+$ fluorescence could be useful in this regard.

ACKNOWLEDGMENTS

The authors are grateful to J. Stickrod and E. Bayarsaikhan for assistance with experiments and to J. McCaffrey, A. Buchachenko, and B. Gervais for helpful discussions of the theory of Ba atoms in noble gas matrix. This material is based upon work supported by the National Science Foundation under Grants No. 2011948 and No. 1649324. The authors gratefully acknowledge support for nEXO from the Office of Nuclear Physics within DOE's Office of Science, and NSF in the United States; from NSERC, CFI, FRQNT, NRC, and the McDonald Institute (CFREF) in Canada; from IBS in Korea; and from CAS and NSFC in China. This work was supported in part by Laboratory Directed Research and Development (LDRD) programs at Brookhaven National

Laboratory (BNL), Lawrence Livermore National Laboratory (LLNL), Oak Ridge National Laboratory (ORNL), Pacific Northwest National Laboratory (PNNL), and SLAC National Accelerator Laboratory.

---

[1] C. Pryor and F. Wilczek, "Artificial vacuum" for T-violation experiment, Phys. Lett. B **194**, 137 (1987).

[2] M. Arndt, S. I. Kanorsky, A. Weis and T. W. Hänsch, Can paramagnetic atoms in superfluid helium be used to search for permanent electric dipole moments? Phys. Lett. A **174**, 298 (1993).

[3] M. G. Kozlov and A. Derevianko, Proposal for a sensitive search for the electric dipole moment of the electron with matrix-isolated radicals, Phys. Rev. Lett. **97**, 063001 (2006).

[4] A. C. Vutha, M. Horbatsch and E. A. Hessels, Oriented polar molecules in a solid inert-gas matrix: A proposed method for measuring the electric dipole moment of the electron, Atoms **6**, 3 (2018).

[5] S. Upadhyay, U. Dargyte, V. D. Dergachev, R. P. Prater, S. A. Varganov, T. V. Tscherbul, D. Patterson, and J. D. Weinstein, Spin coherence and optical properties of alkali-metal atoms in solid parahydrogen, Phys. Rev. A **100**, 063419 (2019).

[6] T. Battard, S. Lahs, C. Crépin, and D. Comparat, Cesium atoms in a cryogenic argon matrix, Phys. Rev. A **108**, 042820 (2023).

[7] C. Braggio *et al.*, Spectroscopy of alkali atoms in solid matrices of rare gases: Experimental results and theoretical analysis, Appl. Sci. **12**, 6492 (2022).

[8] V. Gaire, M. Y. Do, Y. Pei, A. Semenova, and C. V. Parker, High resolution spectroscopy of thulium atoms implanted in solid noble gas crystals, Phys. Rev. B **108**, 214101 (2023).

[9] M. K. Moe, New approach to the detection of neutrinoless double-beta decay, Phys. Rev. C **44**, R931 (1991).

[10] M. Miyajima, S. Sasaki and H. Tawara, Time-of-flight mass spectrometric analysis of daughter isotope of ^{136}Ba in double beta-decay of ^{136}Xe, in *Proceedings of 6th Workshop on Radiation Detectors and Their Uses, Tsukuba, Japan*, KEK Proc. 91-5 (National Laboratory for High Energy Physics, 1991), pp. 19–31.

[11] M. Miyajima, S. Sasaki and H. Tawara, Project for detecting the double beta decay of ^{136}Xe, Hyperfine Interact. **74**, 159 (1992).

[12] M. Miyajima, S. Sasaki and H. Tawara, Search for double beta-decay products of ^{136}Xe in liquid xenon, IEEE Trans. Nucl. Sci. **41**, 835 (1994).

[13] M. Miyajima, S. Sasaki, H. Tawara and E. Shibamura, Application of RIS to search for double beta decay of ^{136}Xe, in *Resonance Ionization Spectroscopy 1996*, AIP Conf. Proc. No. 388 (AIP Press, Woodbury, NY, 1997).

[14] M. Danilov *et al.*, Detection of very small neutrino masses in double-beta decay using laser tagging, Phys. Lett. B **480**, 12 (2000).

[15] M. Miyajima, Studies of barium ion mobility in liquid xenon, in *Proceedings of the International Workshop on Technique and Application of Xenon Detectors, University of Tokyo, Japan, 3–4 December 2001* (World Scientific Pub Co Inc., 2003), p. 115.

[16] T. Shimoyama, E. Shibamura, T. Nishikawa and M. Miyajima, Simulation for determining position and size of laser shots to identify double beta decay daughter in liquid xenon ionization drift chamber, Jpn. J. Appl. Phys. **43**, 8278 (2004).

[17] K. Wamba *et al.*, Mobility of thorium ions in liquid xenon, Nucl. Instrum. Methods Phys. Res., Sect. A **555**, 205 (2005).

[18] B. Flatt *et al.*, A linear RFQ ion trap for the Enriched Xenon Observatory, Nucl. Instrum. Methods Phys. Res., Sect. A **578**, 399 (2007).

[19] S.-C. Jeng, W. M. Fairbank, Jr., and M. Miyajima, Measurements of the mobility of alkaline earth ions in liquid xenon, J. Phys. D: Appl. Phys. **42**, 035302 (2009).

[20] D. Sinclair *et al.*, Prospects for barium tagging in gaseous xenon, J. Phys.: Conf. Ser. **309**, 012005 (2011).

[21] K. Twelker *et al.*, An apparatus to manipulate and identify individual Ba ions from bulk liquid Xe, Rev. Sci. Instrum. **85**, 095114 (2014).

[22] B. Mong *et al.*, Spectroscopy of Ba and Ba^{+} deposits in solid xenon for barium tagging in nEXO, Phys. Rev. A **91**, 022505 (2015).

[23] T. Brunner *et al.*, An RF-only ion-funnel for extraction from high-pressure gases, Int. J. Mass Spectrom. **379**, 110 (2015).

[24] C. Chambers *et al.*, Imaging individual barium atoms in solid xenon for barium tagging in nEXO, Nature (London) **569**, 203 (2019).

[25] H. Rasiwala *et al.*, 'Searching for a needle in a haystack;' A Ba-tagging approach for an upgraded nEXO experiment, Nucl. Instrum. Methods Phys. Res., Sect. B **541**, 298 (2023).

[26] D. R. Nygren, Detection of the barium daughter in $^{136}\text{Xe} \rightarrow {}^{136}\text{Ba} + 2\text{e}^{-}$ by *in situ* single-molecule fluorescence imaging, Nucl. Instrum. Methods Phys. Res., Sect. A **824**, 2 (2016).

[27] B. J. P. Jones, A. D. McDonald and D. R. Nygren, Single molecule fluorescence imaging as a technique for barium tagging in neutrinoless double beta decay, J. Inst. **11**, P12011 (2016).

[28] A. D. McDonald *et al.* (NEXT Collaboration), Demonstration of single-barium-ion sensitivity for neutrinoless double-beta decay using single-molecule fluorescence imaging, Phys. Rev. Lett. **120**, 132504 (2018).

[29] P. Thapa, I. Arnquist, N. Byrnes, A. A. Denisenko, F. W. Foss Jr., B. J. P. Jones, A. D. McDonald, D. R. Nygren and K. Woodruff, Barium chemosensors with dry-phase fluorescence for neutrinoless double beta decay, Sci. Rep. **9**, 15097 (2019).

[30] I. Rivilla *et al.*, Fluorescent bicolour sensor for low-background neutrinoless double β decay experiments, Nature (London) **583**, 48 (2020).

[31] P. Herrero-Gómez *et al.*, Ba^{+2} ion trapping using organic submonolayer for ultra-low background neutrinoless double beta detector, Nat. Commun. **13**, 7741 (2022).

[32] N. Byrnes *et al.* (NEXT Collaboration), Fluorescence imaging of individual ions and molecules in pressurized noble gases for barium tagging in ^{136}Xe, arXiv:2406.15422 [Nat. Commun. (to be published)].

[33] D. M. Lancaster, U. Dargyte, and J. D. Weinstein, Optical spin readout of single rubidium atoms trapped in solid neon, Phys. Rev. Res. **6**, L012048 (2024).

[34] B. Loseth, R. Fang, D. Frisbie, K. Parzuchowski, C. Ugalde, J. Wenzl, and J. T. Singh, Detection of atomic nuclear reaction products via optical imaging, Phys. Rev. C **99**, 065805 (2019).

[35] C. L. Cowan, F. Reines, F. B. Harrison, H. W. Kruse, and A. D. McGuire, Detection of the free neutrino: A confirmation, Science **124**, 103 (1956).

[36] M. J. Dolinski, A. W. P. Poon and W. Rodejohann, Neutrinoless double-beta decay: Status and prospects, Annu. Rev. Nucl. Part. Sci. **69**, 219 (2019).

[37] N. Ackerman *et al.* (EXO Collaboration), Observation of two-neutrino double-beta decay in ^{136}Xe with EXO-200, Phys. Rev. Lett. **107**, 212501 (2011).

[38] J. Albert *et al.* (EXO Collaboration), An improved measurement of the $2\nu\beta\beta$ half-life of ^{136}Xe with EXO-200 detector, Phys. Rev. C **89**, 015502 (2014).

[39] G. Anton *et al.* (EXO-200 Collaboration), Search for neutrinoless double-beta decay with the complete EXO-200 dataset, Phys. Rev. Lett. **123**, 161802 (2019).

[40] G. Adhikari *et al.*, nEXO: Neutrinoless double beta decay search beyond 10^{28} year half-life sensitivity, J. Phys. G: Nucl. Part. Phys. **49**, 015104 (2022).

[41] J. B. Albert *et al.*, Measurements of the ion fraction and mobility of α- and β-decay products in liquid xenon using EXO-200, Phys. Rev. C **92**, 045504 (2015).

[42] B. M. Davis and J. G. McCaffrey, Absorption spectroscopy of heavy alkaline earth metals Ba and Sr in rare gas matrices–CCSD(T) calculations and atomic site occupancies, J. Chem. Phys. **144**, 044308 (2016).

[43] B. M. Davis and J. G. McCaffrey, Luminescence of atomic barium in rare gas matrices: A two-dimensional excitation/emission spectroscopy study, J. Phys. Chem. A **122**, 7339 (2018).

[44] B. M. Davis, B. Gervais and J. G. McCaffrey, An investigation of the sites occupied by atomic barium in solid xenon–A 2D-EE luminescence spectroscopy and molecular dynamics study, J. Chem. Phys. **148**, 124308 (2018).

[45] N. N. Kleshchina, I. S. Kalinina, I. V. Leibin, D. S. Bezrukov, and A. A. Buchachenko, Stable axially symmetric atomic impurity in an fcc solid-Ba in rare gases, J. Chem. Phys. **151**, 121104 (2019).

[46] B. Gervais (private communication).

[47] Meller Optics MSW075/020Z.

[48] B. Davis, Luminescence spectroscopy of strontium and barium atoms isolated in low temperature solids – an experimental and theoretical study, Ph.D. thesis, Maynooth University, 2016.

[49] C. Chambers, Imaging individual barium atoms in solid xenon by scanning of a focused laser for use in the nEXO experiment, Ph.D. thesis, Colorado State University, 2019.

[50] Beam Imaging Solutions model G-2 ion gun.

[51] The exposure quoted in this paper is the laser power measured before the aspherical focusing lens times exposure time divided by the effective laser area $\pi w_x w_y/2$ including vibration compensation.

[52] T. Walton, Imaging single barium atoms in solid xenon for barium tagging in the nEXO neutrinoless double beta decay experiment, Ph.D. thesis, Colorado State University, 2016.

[53] M. Ryan, M. Collier, P. de Pujo, C. Crépin, and J. G. McCaffrey, Investigations of the optical spectroscopy of atomic sodium isolated in solid argon and krypton: Experiments and simulations, J. Phys. Chem. A **114**, 3011 (2010).

[54] L.-G. Tao, N. N. Kleshchina, R. Lambo, A. A. Buchachenko, X.-G. Zhou, D. S. Bezrukov and S.-M. Hu, Heat- and light-induced transformations of Yb trapping sites in an Ar matrix, J. Chem. Phys. **143**, 174306 (2015).

[55] A. A. Buchachenko (private communication).

[56] R. Kometer and N. Schwentner, Light-induced migration of Ag in Xe films and generation of sites, J. Chem. Phys. **104**, 6967 (1996).

[57] A. Steinmetz, A. Schrimpf, H.-J. Stöckmann, E. Görlach, R. Dersch, G. Sulzer and H. Ackermann, Site modification of K atoms in solid Ar by X-ray and light irradiation, Z. Phys. D **4**, 373 (1987).

[58] S. Kravitz, H. Chen, R. Gibbons, S. J. Haselschwardt, Q. Xia and P. Sorensen, Operation and performance of a dual-phase crystalline/vapor xenon time projection chamber, J. Inst. **17**, P04014 (2022).